

AN OPTIMIZATION STUDY OF THE TARGET SUBSYSTEM FOR THE NEW G-2 EXPERIMENT*

C. Yoshikawa[#], C. Ankenbrandt, Muons, Inc., Batavia, IL 60510, USA

A. Leveling, N.V. Mokhov, J. Morgan, D. Neuffer, S. Striganov, Fermilab, Batavia, IL 60510, USA

Abstract

A precision measurement of the muon anomalous magnetic moment, $a_\mu = (g-2)/2$, was previously performed at BNL with a result of 2.2 - 2.7 standard deviations above the Standard Model (SM) theoretical calculations. The same experimental apparatus is being planned to run in the new Muon Campus at Fermilab, where the muon beam is expected to have less pion contamination and the extended dataset may provide a possible 7.5σ deviation from the SM, creating a sensitive and complementary benchmark for proposed SM extensions. We report here on a study performed on the target subsystem utilizing a new optimization technique that overcomes complexities of asymmetric particle production and depth of focus of a Li lens. This new technique is applied to an apparatus that is optimized for pions that have favourable phase space to create polarized daughter muons around the magic momentum of 3.094 GeV/c, which is needed by the downstream g 2 muon ring.

INTRODUCTION

The New g-2 Experiment at Fermilab [1] aims to measure the muon anomalous magnetic moment to a precision of ± 0.14 ppm — a fourfold improvement over the 0.54 ppm precision obtained in the g-2 BNL E821 experiment [2]. The present discrepancy, $\Delta a_\mu(\text{Expt.} - \text{SM}) = (255 \pm 80) \times 10^{-11}$, is already suggestive of possible new physics contributions to the muon anomaly. Assuming that the current theory error of 49×10^{-11} is reduced to 30×10^{-11} on the time scale of the completion of our experiment, a future Δa_μ comparison would have a combined uncertainty of $\approx 34 \times 10^{-11}$, resulting in a 7.5σ deviation from the Standard Model, which will be a sensitive and complementary benchmark for proposed extensions to the Standard Model. Most of the improvement will be due to increased statistics and thus it is essential to maximize production of useful pions that create polarized muons which are in the acceptance of the g-2 muon storage ring. Furthermore, cost considerations favour a design that reuses the existing pbar production subsystem that worked well during the Tevatron operation. Hence, the pion production subsystem will begin with the pbar production subsystem scaled from 8 GeV (kinetic energy) protons to 3.1 GeV/c pions.

A preliminary study [3] revealed complexities in optimizing the target where there is interplay between the asymmetric pion production, the need to have the pions created near the target edges to minimize reabsorption, and the depth of focus of the Li lens. An optimization procedure was proposed in that early study to overcome

those complications and its application and result is the focus of the study reported here.

THE LAYOUT

A graphical representation of the Fermilab pbar production target subsystem is shown in Figure 1 as implemented in Ref. [4] in the MARS15 code [5]. The proton beam with kinetic energy of 8 GeV impinges on the default target, which was previously used to create pbars. We considered two spot sizes for the proton. One is what we expect from a simple scaling from 120 GeV operation to 8 GeV. The other is the smallest we believe that can be achieved. Spot size information on both is provided in Table 1. The default pbar production target is a vertical cylinder (in-out of top view in Figure 1) composed primarily of inconel with a chord for the proton beam of ~ 7.5 cm. Pions produced in the target will be focused by the Li lens (yellow) that is 15 cm long, 1 cm in radius, and has a magnetic field gradient of 256.25 T/m, where the gradient has been scaled for 3.1 GeV/c pions to maintain proper focusing, while keeping the same focusing distance between centers of the target and Li lens of 25.16 cm. The focused pion beam is then collimated and bent through a pulsed magnet (PMAG) with a dipole field of 0.542219 T, also scaled for the 3.1 GeV/c pion beam, and bends the reference by 3 degrees to provide momentum selection.

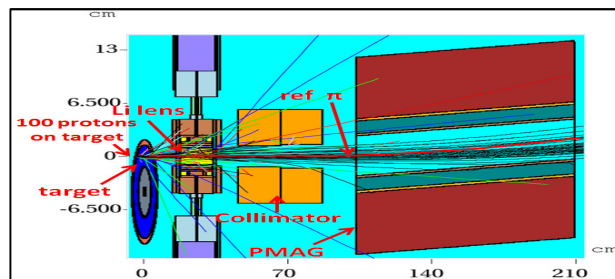


Figure 1: Zoomed in top view of pbar target subsystem.

Table 1: Proton Beam Spot Sizes

Proton spot size description	σ_x (mm)	σ_y (mm)	$\sigma_{x'}$ (mrad)	$\sigma_{y'}$ (mrad)
Default	0.55	1.1066	0.38	0.38
Small	0.15	0.15	0.6366	0.6366

A transition in our simulation between MARS that provides reliable particle generation and G4beamline [6] that is used for particle tracking, pion decay into muons, and effect of beam particles interacting with the beam line elements is shown in Figure 2. The MARS particle tracks that hit the virtual detector are converted and propagated in G4beamline through a set of four quads that refocuses

*Work supported by Fermi Research Alliance, LLC, under contract

No. DE-AC02-07CH11359 with the U.S. Department of Energy

[#]cary.yoshikawa@muonsinc.com

the beam after the three degree bend from the PMAG. Figure 3 shows 100 such particle tracks traversing the four quads.

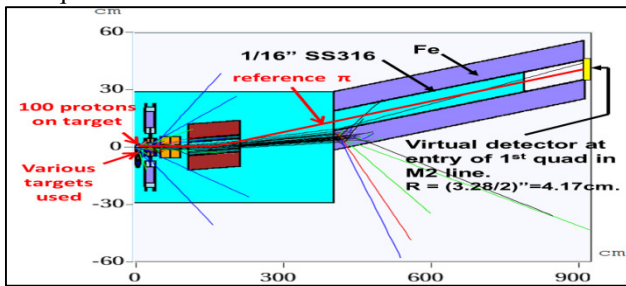


Figure 2: Top view of pbar target subsystem.

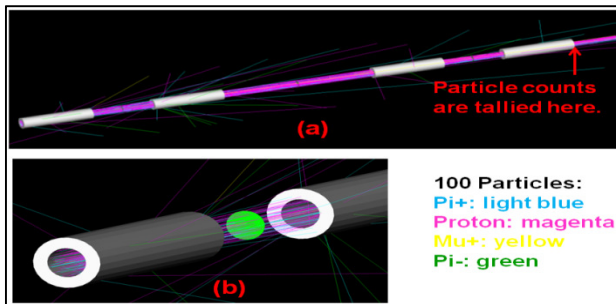


Figure 3: Particles after the conversion into G4beamline and propagated through the 4 quads. (a) Particle yields are tallied at end of the fourth quad with acceptance cuts appropriate for downstream elements. (b) Zoomed in view of particle trajectories between quads that are seen by a virtual detector (green).

The particle yields expected for the g-2 muon ring are estimated by particles simulated to the end of the fourth quad in the Fermilab M2 line as shown in Figure 3(a) and applying the acceptance of those downstream elements, which are:

- $P(\pi^+) = 3.15588 \text{ GeV}/c \pm 2\% (1.02 \times P_{\text{magic}} \pm 0.02 \times P_{\text{magic}})$
- $40\pi \text{ mm-mrad}$ in each transverse dimension

THE OPTIMIZATION

The previous study [3] utilized thin inconel targets of varying widths, lengths (in direction of proton beam), and orientations (vertical and horizontal). In the current study, we assume pions emanating from the surface in the non-bend plane will give better yields downstream, so we considered only the horizontal orientation. Application of the horizontal slab target into a more realistic one that incorporates cooling would be via a rotating thin walled cylinder with the proton beam hitting either the top or bottom, as shown in Figure 4.

The earlier study also fixed the location of the target center to be at the focal point of the Li lens, while varying the target dimensions. Since pion production is greatest at the upstream end of the target, lengthening the target pushes the location of copious pion production ahead and out of the focal point of the Li lens. The solution to overcome the complexity between varying the target geometry and maintaining focus is to recognize that there

will be much less useful pions produced at the downstream end of a long flat target. The procedure involves two stages, where the first optimizes for the location of the upstream edge of the target which is more critical, since that is where pion production is copious. It consists of the following steps as illustrated in Figure 5:

1. Placing the downstream end of a horizontal flat target far downstream as possible, near to the Li lens.
2. The upstream end of the target will be varied starting from the focal point and progressed upstream in each simulated configuration.

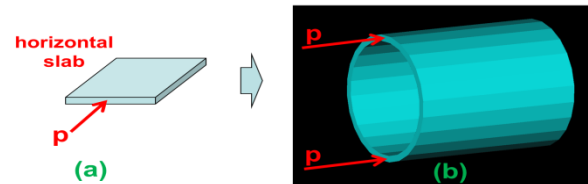


Figure 4: Association of simulated horizontal slab targets and a more practical rotating thin walled cylindrical target to accommodate cooling where protons impinge on either the top or bottom of the cylinder.

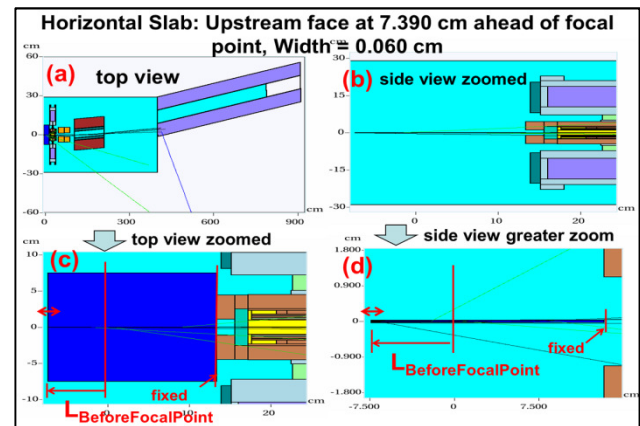


Figure 5: Illustration of optimization for location of upstream target edge. The downstream edge is fixed near the Li lens. The top view is shown in (a) which is similar to that shown in Fig. 2 for the default target. A zoomed in side view is shown in (b), while (d) is further zoomed to show the variation of upstream edge location relative to the Li lens focal point and (c) is similar for the top view.

The geometry of the targets studied, which included varying widths, are given in Table 2 and the anticipated small proton beam spot size described in Table 1 was used throughout the optimization. Results of this first stage of optimization are shown in Figure 6, where it is seen that there are two optimal configurations which provide similar yields:

- $L_{\text{BeforeFocalPoint}} = 56.12 \text{ mm}$ & width = 0.60 mm
- $L_{\text{BeforeFocalPoint}} = 66.79 \text{ mm}$ & width = 0.75 mm

Both configurations will be carried forward into the second stage of optimization.

Table 2: Dimensions and Orientations of Targets Studied. Material of all targets is inconel.

Shape	$L_{\text{BeforeFocalPoint}}$ (mm)	Width (mm)
Horizontal Slab	0, 36.95, 73.9, 110.85 λ_{int} : 0, 0.25, 0.50, 0.75	0.60, 0.75, 1.00, 1.25
Default Pbar Target	chord ~75 mm	

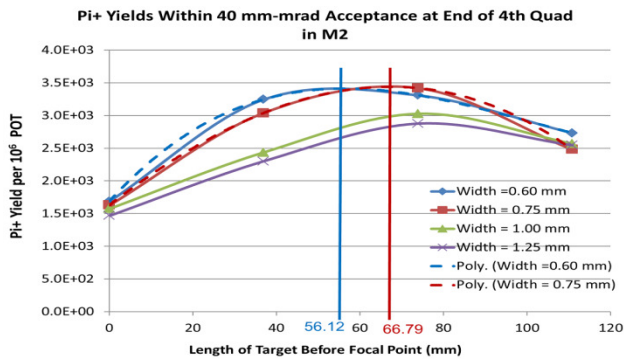


Figure 6: Yield of π^+ s in first stage of optimization for location of upstream target edge.

The second stage of optimization consists of simply trimming the downstream end of the target; this automatically maximizes the yield taking into account the effects of:

- Widening birth of pions nearer the surface due to growth of transverse proton beam size as it traverses the target.
- Pions produced near the downstream edge.

The procedure for this second stage of optimization is to fix the location of the upstream edge of the target at locations determined from the first stage and vary the target length. Figure 7 illustrates this procedure for one of the optimal cases elucidated in the first stage.

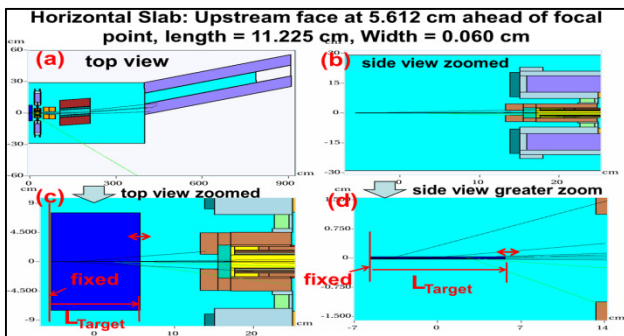


Figure 7: Illustration of optimization for location of downstream target edge. The upstream edge is fixed according to a result of first stage, while the downstream edge is varied. The top view is shown in (a) which is similar to that shown in Fig. 2 for the default target. A zoomed in side view is shown in (b), while (d) is further zoomed to show the variation of the downstream edge location and (c) is similar from the top view.

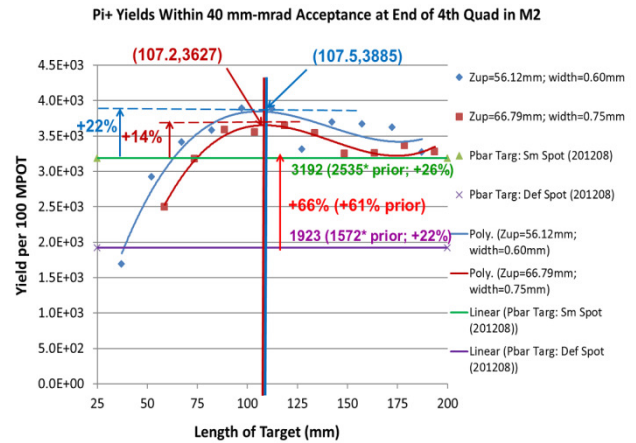


Figure 8: Yield of π^+ s in second stage of optimization for location of downstream target edge. Values designated “prior” refer to results obtained from MARS version 1510 used in the previous study [3], while the current results (also designated 201208) utilized MARS version 1512.

Results of the second stage of optimization as well as the effect of reducing the proton beam spot size on the default pbar target are shown in Figure 8. It is seen that the reduction of the proton beam spot size on the default pbar target increases the yield of useful pions by 66%! The optimized horizontal slab target using the same small proton beam spot size increases it further by 22%. While an increase of 22% is non-trivial, a cost-benefit and risk analysis resulted in the decision to keep the default pbar target design and reap the large benefit of the anticipated smaller proton beam size.

ACKNOWLEDGMENT

The support, encouragement, and contributions of Chris Polly, Mary Convery, and Dean Still of Fermilab are gratefully acknowledged.

SUMMARY

A study of the New g-2 Experiment target system at Fermilab was performed to optimize the yield of useful pions. An optimization procedure was invented that overcame the complexities of an asymmetric particle production and depth of focus of a Li lens. The best possible target modification yielded a 22% increase over that of the default pbar target and a cost-benefit decision was made by the New g-2 collaboration to resuse the existing pbar target design.

REFERENCES

- [1] R. M. Carey et al., http://gm2.fnal.gov/public_docs/proposals/Proposal-APR5-Final.pdf
- [2] G. W. Bennett et al., Phys. Rev. D 73 (2006) 072003.
- [3] C. Yoshikawa et al., “Optimization of the Target Subsystem for the New g-2 Experiment,” IPAC12 MOPPD044.
- [4] N. Mokhov, g-2 collaboration meeting note (2009).
- [5] MARS: N. Mokhov, <http://www-ap.fnal.gov/MARS>
- [6] G4beamline: T. Roberts, <http://g4beamline.muonsinc.com>